A Study of Non-Smooth Convex Flow Decomposition

Jing Yuan, Christoph Schnörr, Gabriele Steidl, Florian Becker
University of Mannheim
Dept. Mathematics and Computer Science
-68131 Mannheim, Germany

Abstract

We present a mathematical and computational feasibility study of the variational convex decomposition of 2D vector fields into coherent structures and additively superposed flow textures. Such decompositions are of interest for the analysis of image sequences in experimental fluid dynamics and for highly non-rigid image flows in computer vision.

Our work extends current research on image decomposition into structural and textural parts in a twofold way. Firstly, based on Gauss' integral theorem, we decompose flows into three components related to the flow's divergence, curl, and the boundary flow. To this end, we use proper operator discretizations that yield exact analogs of the basic continuous relations of vector analysis. Secondly, we decompose simultaneously both the divergence and the curl component into respective structural and textural parts. We show that the variational problem to achieve this decomposition together with necessary compatibility constraints can be reliably solved using a single convex second-order conic program.

1. Introduction

The representation, estimation, and analysis of non-rigid motions is relevant to many scenarios in computer vision, medical imaging, remote sensing, and experimental fluid dynamics. In the latter case, for example, sophisticated measurement techniques including pulsed laser light sheets, modern CCD cameras and dedicated hardware, enable the recording of high-resolution image sequences that reveal the evolution of spatial structures of unsteady flows [14].

In this context, two issues are particularly important. Firstly, the design and investigation of variational approaches to motion estimation that are well-posed through regularization but do not penalize relevant flow structures are of interest. A corresponding line of research concerns the use of higher-order regularizers as investigated, for example, in [16, 5, 9]. Secondly, representation of motions by components that capture different physical aspects are important for most areas of application mentioned above. Referring again to experimental fluid dynamics, for example, the extraction of coherent flow structures which are immersed into additional motion components at different spatial scales [10], poses a challenge for image sequence analysis.

The decomposition of images has become an interesting and active area of research quite recently. Based on the seminal paper [15] introducing total variation based image denoising, and on the use of norms that are suited for representing oscillating patterns [12], a range of novel variational and computational approaches have been suggested for decomposing images of general scenes into basic components related to geometry, texture, and noise; e.g., [17, 18, 1, 2].

In the present paper, we focus on function decomposition from the viewpoint of non-rigid variational motion analysis. Specifically, we consider Meyer's [12] variational model

$$\min \mathrm{TV}(f^s)\,, \quad \text{s.t.} \quad f^s + f^t = f\,,\ \left\|f^t\right\|_G \leq \delta \qquad (1)$$

as a representative approach to the decomposition of a function f into its basic structural and textural parts f^s, f^t, and study the feasibility of an extension to the decomposition of motion vector fields. Our objective consists is the *simultaneous* decomposition of a vector field into physically relevant components related to its divergence and curl, *and* the decomposition of these components into parts with intrinsic variations at different scales.

In section 2, we introduce the discrete representation of vector fields by its basic components related to divergence, curl, and boundary values. Based on an accurate discretization employing various finite-dimensional spaces and corresponding operators, a variational model for the simultaneous decomposition of these components is proposed in section 3. From the computational point of view, we prefer to reformulate our variational problem as a convex conic program in subsection 4 because all compatibility constraints defining our decomposition can be included at once. While conic programming has found widespread applications in all branches of computational science, it has only recently

been suggested for the decomposition of scalar-valued image functions [19]. Numerical experiments demonstrate the feasibility of our approach in section 5.

2. Vector Field Representation

2.1. Flow Discretization

For discretizing the relevant differential operators we apply the *mimetic finite difference method* introduced by Hyman and Shashkov in [8]. This method preserves the integral identities satisfied by the continuous differential operators by appropriately defining their discrete analogues simultaneously with respect to two grids which we call primal and dual grid. Then we define

H_P: space of scalar fields on vertices,
H_V: space of scalar field on cells,
H_S: space of vector fields defined normal to sides,
H_E: space of vector fields defined tangential to sides

and H_P^o, H_S^o, H_E^o as their restricted versions of inner scalar/vector fields, see Fig. 1. Likewise we consider the restriced spaces H_P^o, H_S^o, H_E^o also as naturally embedded in H_P, H_S, H_E with zero boundaries. While H_P and H_V are equipped with the usual Euclidian norm, the norms on H_S and H_E include boundary weights, see appendix. Now the discrete versions of the first order operators ∇, div and curl with respect to the primal and dual grid are given by

$$\mathbb{G} : H_P \to H_E,\ \mathbb{D}iv\ : H_S \to H_V,\ \mathbb{C}url\ : H_E \to H_V,$$
$$\overline{\mathbb{G}} : H_V \to H_S,\ \overline{\mathbb{D}iv}\ : H_E^o \to H_P^o,\ \overline{\mathbb{C}url}\ : H_S^o \to H_P^o.$$

Reshaping the scalar/vector fields columnwise into vectors of appropriate lengths, our first-order operators act on the corresponding vector spaces as the matrices in the appendix.

Finally, for discretizing $\mathrm{n}\cdot u|_{\partial\Omega}$, we introduce the boundary operator

$$\mathbb{B}_\mathrm{n} : H_S \to \partial H_S := H_S \backslash H_S^o,$$

which restricts the vector field to the vectors at the grid's boundary multiplied by the outer normal vectors. For the matrix form of the operator see the appendix.

2.2. Flow Representation

For the flow vectors $u \in H_S$, we see by definition of $\mathbb{D}iv$ and $\mathbb{B}_\mathrm{n}$ that

$$\mathbf{1}_{\dim H_V}^\mathrm{T}\, \mathbb{D}iv\ u = \mathbf{1}_{\dim \partial H_S}^\mathrm{T}\, \mathbb{B}_\mathrm{n} u, \tag{2}$$

where $\mathbf{1}_n$ denotes the vector consisting of n ones. This is just the discrete version of the *Gaussian Integral Theorem*

$$\int_\Omega \mathrm{div}\, u \,\mathrm{d}x = \int_{\partial\Omega} n \cdot u \,\mathrm{d}l$$

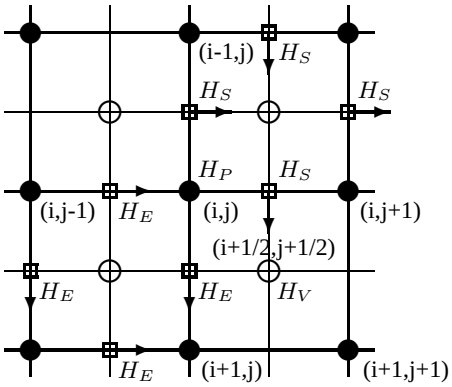

Figure 1. Spaces H_P, H_V, H_S and H_E.

Conversely, we say that $\rho \in H_V$ and $\nu \in \partial H_S$ fulfill the *compatibility condition* if

$$\mathbf{1}_{\dim H_V}^\mathrm{T}\, \rho = \mathbf{1}_{\dim \partial H_S}^\mathrm{T}\, \nu \tag{3}$$

Besides the flow representation $u \in H_S$, we will apply a second flow representation. To this end, consider the operator $A : H_S \to H_V \oplus H_P^o \oplus \partial H_S$ given in matrix form by

$$A := \begin{pmatrix} \mathbb{D}iv \\ \overline{\mathbb{C}url} \\ \mathbb{B}_\mathrm{n} \end{pmatrix} \in \mathbb{R}^{\dim H_S + 1, \dim H_S}\ , \tag{4}$$

where the $\overline{\mathbb{C}url}$ operator is naturally extended to the whole space H_S here. The operator A has full rank $\dim H_S$. Moreover, we see by (2) that $(\rho, \omega, \nu)^\mathrm{T}$ is in the image of A iff ρ and ν fulfill the compatibility condition (3). In this case u can be obtained from given $(\rho, \omega, \nu)^\mathrm{T}$ by $u = A^\dagger(\rho, \omega, \nu)^\mathrm{T}$, where $A^\dagger = (A^\mathrm{T}A)^{-1}A^\mathrm{T}$ denotes the pseudoinverse of A.

Proposition 1 *There exists a one–to–one correspondence between the spaces H_S and*

$$V_S := \{(\rho, \omega, \nu)^T : \mathbf{1}_{\dim H_V}^T\, \rho = \mathbf{1}_{\dim \partial H_S}^T\, \nu\}\ ,$$

where $\rho = \mathbb{D}iv\ u$, $\omega = \overline{\mathbb{C}url}\, u$, $\nu = \mathbb{B}_\mathrm{n} u$ and conversely $u = A^\dagger(\rho, \omega, \nu)^T$.

3. Variational Approaches

3.1. Flow Decomposition

In this section, we want to decompose flow vectors $u \in H_S$, resp., $(\rho, \omega, \nu)^\mathrm{T} \in V_S$ in a meaningful way. To this end, let c_ρ denote the mean of the divergence of u and c_ω the mean of the curl of u, i.e.,

$$c_\rho := \mathbf{1}_{\dim H_V}^\mathrm{T}\, \rho \,/\, \dim H_V = \mathbf{1}_{\dim H_V}^\mathrm{T}\, \mathbb{D}iv\ u \,/\, \dim H_V \tag{5}$$
$$c_\omega := \mathbf{1}_{\dim H_P^o}^\mathrm{T}\, \omega \,/\, \dim H_P^o = \mathbf{1}_{\dim H_P^o}^\mathrm{T}\, \mathbb{C}url\ u \,/\, \dim H_P^o \tag{6}$$

These are the discrete versions of $|\Omega|^{-1}\int_\Omega \operatorname{div}(u)dx$ and $|\Omega|^{-1}\int_\Omega \operatorname{curl}(u)dx$. Then we can decompose the flow $(\rho,\omega,\nu)^{\mathrm{T}} \in V_S$ as

$$(\rho,\omega,\nu) = (c_\rho, c_\omega, \nu) + (\rho^o, \omega^o, 0), \tag{7}$$

where $\mathbf{1}^{\mathrm{T}}_{\dim H_V}\rho_o = \mathbf{1}^{\mathrm{T}}_{\dim H^o_P}\omega_o = 0$. Obviously, we have that $(c_\rho, c_\omega, \nu)^{\mathrm{T}}, (\rho^o, \omega^o, 0)^{\mathrm{T}} \in V_S$ again, so that

$$u = u^c + u^o$$

is the corresponding decomposition of $u \in H_S$, where $u^c := A^\dagger(c_\rho, c_\omega, \nu)^{\mathrm{T}}$ and $u^o := A^\dagger(\rho^o, \omega^o, 0)^{\mathrm{T}}$. The vector u^c, resp. (c_ρ, c_ω, ν), represents the basic pattern of the non-rigid flow and its boundary behaviour while u^o, resp. $(\rho^o, \omega^o, 0)$, is related to the variant flow pattern. Now we want to further decompose the intrinsic flow variation u^o into a structural part u^s and a texture part u^t, i.e.,

$$u^o = u^s + u^t.$$

By proposition 1 this corresponds to the decomposition

$$(\rho^o, \omega^o, 0) = (\rho^s, \omega^s, 0) + (\rho^t, \omega^t, 0).$$

In summary, our task consists in the decomposition of a given flow field $u \in H_S$ as

$$u = u^c + u^s + u^t. \tag{8}$$

We can apply A to u which provides us by using in addition (5) and (6) with $(c_\rho, c_\omega, \nu)^{\mathrm{T}}$ and $(\rho^o, \omega^o, 0)^{\mathrm{T}}$. Then, inspired by Meyer's approach (1), we may compute $(\rho^s, \omega^s, 0)$ and $(\rho^t, \omega^t, 0)$ as solutions of the minimization problem

$$\begin{aligned} J(\rho^s, \omega^s, \rho^t, \omega^t) &= \lambda_d \mathrm{TV}(\rho^s) + \lambda_c \mathrm{TV}(\omega^s), \qquad (9)\\ \text{s.t.}\quad & \rho^s + \rho^t = \rho^o,\ \omega^s + \omega^t = \omega^o,\\ & \left\|\rho^t\right\|_G \le \delta_d\,, \quad \left\|\omega^t\right\|_G \le \delta_c, \end{aligned}$$

where the discrete TV functionals and the discrete versions of the G norm are defined in the appendix. This variational approach extends Meyer's model for the decomposition of scalar-valued functions to the *simultaneous* decomposition of vector fields into basic flow patterns. Finally, we may formally obtain u^s and u^t by solving the linear systems $(A^{\mathrm{T}}A)u^s = A^{\mathrm{T}}(\rho^s, \omega^s, 0)^{\mathrm{T}}$ and $(A^{\mathrm{T}}A)u^t = A^{\mathrm{T}}(\rho^t, \omega^t, 0)^{\mathrm{T}}$. However, these systems are very ill-conditioned so that we prefer to compute the components of u directly by minimizing the corresponding functional

$$\begin{aligned} J(u^c, u^s, u^t) &= \lambda_d \mathrm{TV}(\mathbb{D}iv\ u^s) + \lambda_c \mathrm{TV}(\overline{\mathbb{C}url}\ u^s), \quad (10)\\ \text{s.t.}\quad & u^c + u^s + u^t = u,\\ & \overline{\mathbb{G}}\mathbb{D}iv\ u^c = 0, \quad \mathbb{G}\overline{\mathbb{C}url}\ u^c = 0,\\ & \mathbf{1}^{\mathrm{T}}_{\dim H^o_P}\overline{\mathbb{C}url}\ u^s = 0,\\ & \mathbb{D}iv\ u^t = \rho^t,\ \overline{\mathbb{C}url}\ u^t = \omega^t,\\ & \left\|\rho^t\right\|_G \le \delta_d\,, \quad \left\|\omega^t\right\|_G \le \delta_c. \end{aligned}$$

This approach also fits into our flow estimation model in the next section. We note that the third constraint is related to the decomposition (7). While $\mathbf{1}^{\mathrm{T}}_{\dim H_V}\mathbb{D}iv\ u^o = 0$ is automatically fulfilled by the compatibility condition, we have to take care about $\mathbf{1}^{\mathrm{T}}_{\dim H^o_P}\overline{\mathbb{C}url}\,u^o = 0$. However, by the G norm constraint we have that $\overline{\mathbb{C}url}\,u^t = \mathbb{D}iv\,p$ which again by the compatibility condition and since $\overline{\mathbb{C}url}$ maps to H^o_P implies that $\mathbf{1}^{\mathrm{T}}_{\dim H^o_P}\overline{\mathbb{C}url}\,u^t = 0$ so that we have only to take u^s into account.

Finally, we point out that as in the scalar-valued case, some variations of the approach (10) are easily conceivable. Referring to [17, 1], for instance, the constraint $u^c + u^s + u^t = u$ in (10) could be replaced by a L^2 penalty term. Again, this would imply L^2 penalty terms for each component in the decomposition.

3.2 Optical Flow Estimation through Flow Decomposition

In this section, we combine the usual optical flow estimation method with the structure-texture flow decomposition (8). For a given image sequence $\{g\} \in H_V$, we want to compute the components u^c with constant divergence and curl, the large-scale patterns u^s of divergence and curl with bounded BV-norms, and the small-scale patterns u^t of divergence and curl with bounded G-norms by solving

$$\begin{aligned} J(u^c, u^s, u^t) &= \left\|\overline{\mathbb{G}}g \cdot (u^c + u^s + u^t) + g_t\right\|_2^2 \qquad (11)\\ &\quad + \lambda_d \mathrm{TV}(\mathbb{D}iv\ u^s) + \lambda_c \mathrm{TV}(\overline{\mathbb{C}url}\,u^s),\\ \text{s.t.}\quad & \overline{\mathbb{G}}\mathbb{D}iv\ u^c = 0, \quad \mathbb{G}\overline{\mathbb{C}url}\,u^c = 0,\\ & \mathbf{1}^{\mathrm{T}}_{\dim H^o_P}\overline{\mathbb{C}url}\,u^s = 0,\\ & \mathbb{D}iv\ u^t = \rho^t,\ \overline{\mathbb{C}url}\,u^t = \omega^t,\\ & \left\|\rho^t\right\|_G \le \delta_d\,, \quad \left\|\omega^t\right\|_G \le \delta_c. \end{aligned}$$

Here g_t denotes the discretization of the time derivative by a forward difference and the dotproduct is taken with respect to H_S. We refer to (11) as TV–G model. However, for the image areas, where $\nabla g = 0$, the data term disappears such that the local constraints on the two G-norm will lead to infinite solutions. Hence the flow estimation by solving problem (11) is not well-posed. Therefore, we propose the replace the TV–G model by a TV–L_2 model where the texture flow patterns u^t have divergence and curl with bounded L_2-norms:

$$\begin{aligned} J(u^c, u^s, u^t) &= \left\|\overline{\mathbb{G}}g \cdot (u^c + u^s + u^t) + g_t\right\|_2^2 \qquad (12)\\ &\quad + \lambda_d \mathrm{TV}(\mathbb{D}iv\ u^s) + \lambda_c \mathrm{TV}(\overline{\mathbb{C}url}\,u^s)\\ &\quad + \gamma_d \left\|\mathbb{D}iv\ u^t\right\|_2^2 + \gamma_c \left\|\overline{\mathbb{C}url}\,u^t\right\|_2^2, \end{aligned}$$

$$
\begin{aligned}
\text{s.t.}\quad & \overline{\mathbb{G}}\mathbb{D}iv\, u^c = 0, \quad \mathbb{G}\overline{\mathbb{C}url}\, u^c = 0,\\
& \mathbf{1}^{\mathrm{T}}_{\dim H^o_P}(\overline{\mathbb{C}url}\, u^s + \overline{\mathbb{C}url}\, u^t) = 0,\\
& \mathbb{D}iv\ u^t = \rho^t,\ \overline{\mathbb{C}url}\ u^t = \omega^t,\\
& \left\|\rho^t\right\|_G \le \delta_d\,, \quad \left\|\omega^t\right\|_G \le \delta_c.
\end{aligned}
$$

We will see in our experiments that this approach works well although the superiosity of the G–norm over the L_2–norm in capturing (scalar) oszillating patterns was experimentally shown in [3].

3.3 Incompressible Optical Flow Estimation

Incompressible flows which are divergence-free are very common in computational fluid dynamics and 2D turbulence. According to the Helmholtz decomposition, a 2D vector field can be decomposed into an irrotational part and a soleniodal part which is divergence–free. The discete counterpart of the Helmholtz decomposition with respect to our mimetic finite difference discretization can be found in [anonymous]. In particular, we obtain that a divergence-free vector $u \in H_S$ can be written as $u = \mathbb{G}^{\perp}\psi$ for some $\psi \in H_P$, where the operator $\mathbb{G}^{\perp} : H_P \to H_S$ is defined in the appendix. By definition of $\mathbb{G}^{\perp}$ is easy to check that $\mathbb{D}iv\ \mathbb{G}^{\perp} = \mathbf{0}$ and that the restricted operator $\mathbb{G}^{\perp}|_{H^o_P}$ maps to H^o_S. Now we want to estimate the components u^c, u^s and u^t of a divergence–free flow $u = \mathbb{G}^{\perp}\psi$, i.e.,

$$
u = u^c + u^s + u^t = \mathbb{G}^{\perp}\psi^c + \mathbb{G}^{\perp}\psi^s + \mathbb{G}^{\perp}\psi^t, \qquad (13)
$$

where, by regarding the boundary conditions, $\psi^c \in H_P$ and $\psi^s, \psi^t \in H^o_P$. Let $\triangle_c := \overline{\mathbb{C}url}\, \mathbb{G}^{\perp}|_{H^o_P} : H^o_P \to H^o_P$ and $\triangle := \overline{\mathbb{C}url}\, \mathbb{R}^{H_S}_{H^o_S} \mathbb{G}^{\perp} : H_P \to H^o_P$, where $R^{H_S}_{H^o_S}$ denotes the restriction of H_S to H^o_S by boundary cutting. Then we can rewrite our TV–G approach (11) with respect to (13) as

$$
\begin{aligned}
J(\psi^c, \psi^s, \psi^t) = & \left\|\overline{\mathbb{G}}g \cdot \mathbb{G}^{\perp}(\psi^c + \psi^s + \psi^t) + g_t\right\|_2^2 \\
& + \lambda_c \mathrm{TV}(\triangle_c \psi^s) \qquad (14)\\
\text{s.t.}\quad & \mathbb{G}\triangle\psi^c = 0,\ \mathbf{1}^{\mathrm{T}}_{\dim H_P}\psi^c = 0,\\
& \mathbf{1}^{\mathrm{T}}_{\dim H^o_P}\triangle_c\psi^s = 0,\\
& \triangle_c\, \psi^t = \omega^t,\ \left\|\omega^t\right\|_G \le \delta_c,
\end{aligned}
$$

and our TV–L_2 approach (12) as

$$
\begin{aligned}
J(\psi^c, \psi^s, \psi^t) = & \left\|\overline{\mathbb{G}}g \cdot \mathbb{G}^{\perp}(\psi^c + \psi^s + \psi^t) + g_t\right\|_2^2 \\
& + \lambda_c \mathrm{TV}(\triangle_c \psi^s) + \gamma_c \left\|\triangle_c \psi^t\right\|_2^2 \qquad (15)\\
\text{s.t.}\quad & \mathbb{G}\triangle\psi^c = 0,\ \mathbf{1}^{\mathrm{T}}_{\dim H_P}\psi^c = 0,\\
& \mathbf{1}^{\mathrm{T}}_{\dim H^o_P}(\triangle_c\psi^s + \triangle_c\psi^t) = 0.
\end{aligned}
$$

We will see that in areas where $\|\nabla g\| \ll 1$ the solution of (14) becomes sensitive to small pertubations while (15) gives reasonable results.

4. Optimization

Our computational approach to solving (10) is based on second-order cone programming (SOCP) [11]. This amounts to minimizing a linear objective function subject to the constraints that several affine functions of the variables have to lie in a *second order cone* $\mathcal{L}^{n+1} \subset \mathbb{R}^{n+1}$ defined by the convex set

$$
\mathcal{L}^{n+1} = \left\{ \begin{pmatrix} x \\ t \end{pmatrix} = (x_1, \ldots, x_n, t)^{\top} \;\middle|\; \|x\|_2 \le t \right\}. \qquad (16)
$$

With this notation, the general form of a SOCP is given by

$$
\inf_{x \in \mathbb{R}^n} f^{\top} x\,, \ \text{s.t.} \ \begin{pmatrix} A_i x + b_i \\ c_i^T x + d_i \end{pmatrix} \in \mathcal{L}^{n+1}\,,\ i = 1, \ldots, m. \qquad (17)
$$

Problem (17) is a convex program for which efficient, large scale solvers are available [13]. In connection with TV–based image decomposition the application of SOCPs was recently suggested in [19].

Using the notation given in the appendix, we reformulate the variational approach (10) as a SOCP:

$$
\begin{aligned}
& J(u^c, u^s, u^t) = \lambda_d \mathbf{1}^{\mathrm{T}}_{\dim H_V} \boldsymbol{v} + \lambda_c \mathbf{1}^{\mathrm{T}}_{\dim H^o_P} \boldsymbol{w} \qquad (18)\\
& \text{s.t. } u^c + u^s + u^t = u\,, \quad \overline{\mathbb{G}}\mathbb{D}iv\, u^c = 0\,,\ \mathbb{G}\overline{\mathbb{C}url}\, u^c = 0\\
& \mathbf{1}^{\mathrm{T}}_{\dim H^o_P}\overline{\mathbb{C}url}\, u^s = 0\,, \quad \mathbb{D}iv\, u^t = \mathbb{D}iv\, p_d\,,\ \overline{\mathbb{C}url}\, u^t = \mathbb{D}iv\, p_c\\
& \begin{pmatrix} (\overline{\mathbb{G}}\mathbb{D}iv\, u^s)_{V_{i,j}} \\ v_{V_{i,j}} \end{pmatrix} \in \mathcal{L}^5\,,\ \begin{pmatrix} (\overline{\mathbb{G}\mathbb{C}url}\, u^s)_{P^o_{i,j}} \\ w_{P^o_{i,j}} \end{pmatrix} \in \mathcal{L}^5\\
& \begin{pmatrix} (p_d)_{V_{i,j}} \\ \delta_d \end{pmatrix} \in \mathcal{L}^5\,,\ \begin{pmatrix} (p_c)_{P^o_{i,j}} \\ \delta_c \end{pmatrix} \in \mathcal{L}^5
\end{aligned}
$$

In order to incorporate the quadratic terms of the variational approaches to optical flow estimation (11), (12), (14), and (15), we use the following rotated version of the standard cone:

$$
\begin{aligned}
\mathcal{R}^{n+2} := \Big\{ & (\boldsymbol{x}, x_{n+1}, x_{n+2})^{\top} \in \mathbb{R}^{n+2}\,,\\
& x_{n+1} x_{n+2} \ge \frac{1}{2}\|\boldsymbol{x}\|^2\,,\ x_{n+1} + x_{n+2} \ge 0 \Big\}
\end{aligned}
$$

Fixing $x_{n+2} = 1/2$, we have $x_{n+1} \ge \|\boldsymbol{x}\|^2$. Below, we confine ourselves to rewriting (14), and (15) as SOCPs. The SOCPs corresponding to (11), (12) look very similar.

The incompressible flow estimation approach (14), rewritten as a SOCP, reads

$$
\begin{aligned}
& J(\psi^c, \psi^s, \psi^t) = v + \lambda_c \mathbf{1}^{\mathrm{T}}_{\dim H^o_P} \boldsymbol{w} \qquad (19)\\
& \text{s.t.} \quad \mathbb{G}\triangle\psi^c = 0\,,\ \mathbf{1}^{\mathrm{T}}_{\dim H_P}\psi^c = 0\\
& \mathbf{1}^{\mathrm{T}}_{\dim H^o_P}\triangle_c\psi^s = 0\,,\ \triangle_c\psi^t = \mathbb{D}iv\, p_c\\
& \begin{pmatrix} (\overline{G}\triangle_c\psi^s)_{V_{i,j}} \\ w_{V_{i,j}} \end{pmatrix} \in \mathcal{L}^5\,,\ \begin{pmatrix} (p_c)_{P^o_{i,j}} \\ \delta_c \end{pmatrix} \in \mathcal{L}^5
\end{aligned}
$$

$$\begin{pmatrix} \overline{\mathbb{G}}g \cdot \mathbb{G}^{\perp}(\psi^c + \psi^s + \psi^t) + g_t \\ v \\ 1/2 \end{pmatrix} \in \mathcal{R}^{\dim H_V + 2}$$

Approach (15), on the other hand, becomes

$$J(\psi^{c,s,t}) = v + \gamma_d t + \lambda_c \mathbf{1}^{\mathrm{T}}_{\dim H_P^o} \boldsymbol{w} \qquad (20)$$

$$\text{s.t.} \quad \mathbb{G}\triangle\psi^c = 0\,,\ \mathbf{1}^{\mathrm{T}}_{\dim H_P}\psi^c = 0$$

$$\mathbf{1}^{\mathrm{T}}_{\dim H_P^o}\triangle_c\psi^s = 0\,,\ \mathbf{1}^{\mathrm{T}}_{\dim H_P^o}\triangle_c\psi^t = 0$$

$$\begin{pmatrix} (\overline{G}\triangle_c\psi^s)_{V_{i,j}} \\ w_{V_{i,j}} \end{pmatrix} \in \mathcal{L}^5$$

$$\begin{pmatrix} \overline{\mathbb{G}}g \cdot \mathbb{G}^{\perp}(\psi^c + \psi^s + \psi^t) + g_t \\ v \\ 1/2 \end{pmatrix} \in \mathcal{R}^{\dim H_V + 2}$$

$$\begin{pmatrix} \triangle_c\psi^t \\ t \\ 1/2 \end{pmatrix} \in \mathcal{R}^{\dim H_P^o + 2}$$

5. Numerical Experiments

In this section, we will show some experiments on flow decomposition and flow restoration.

Flow Decomposition. Figure 2 shows a turbulent flow field u as ground truth, along with its divergence ρ and curl ω. Figures (3) and (2) show the variational decomposition computed with the approach (10). Note that the structural and textural components recovered the interesting motion patterns at different scales, which are not easily visible in the flow u itself. The decomposed velocties are shown in the following Fig. (4).

Flow Estimation. In this section we will validate the flow estimation models (14) and (15). We first created a divergence-free ground truth flow field u by superimposing a dominant laminar flow (both divergence- and curl-free) with some turbulent vortices structures, see Fig. 5. Using this flow, an artificial image sequence was created for which $|\nabla g(x)| \neq 0,\ \forall x \in \Omega$.

Figures 6, 7 and 8 show the decomposition-based optical flow estimates. The u^c component nicely recovered the laminar flow, whereas the structural and textural components reveal the turbulent curl field. Furthermore, the $\mathrm{TV} - L_2$ regularizer turned out to be more robust than the $\mathrm{TV} - G$ model in connection with the degenerate data term commonly used for variational optical flow estimation.

6. Conclusion and Further Work

Along the lines of current research on variational convex decomposition of image functions, we presented a range of variational models extended to the decomposition and estimation of vector fields which represent image motions. Using proper discretizations, these models achieve a twofold decomposition: three components of the flow field representing flow variations at different scales, along with a further decomposition of the divergence and the curl into a structural and a textural part, respectively. We also pre-

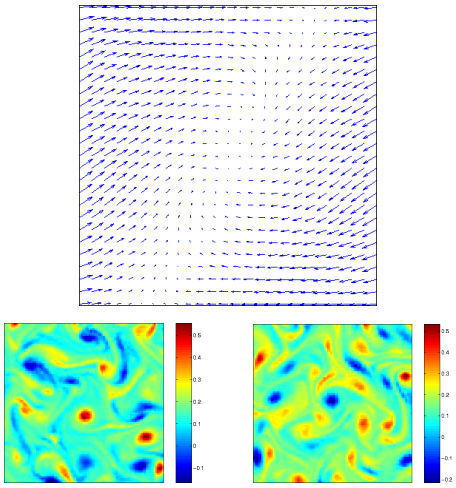

Figure 2. Ground truth data to be decomposed: flow field u (top), its divergence field ρ (bottom, left), and its curl field ω (bottom, right).

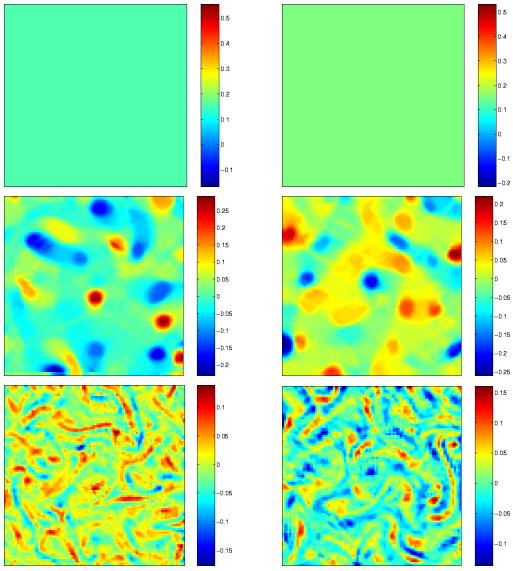

Figure 3. Decomposition of u from Fig. 2 with the approach (10). From top to bottom. Left: ρ^c, ρ^s, ρ^t. Right: $\omega^c, \omega^s, \omega^t$. The structure and texture components reveal turbulent flow patterns at different scales which are not easily visible in the flow u itself.

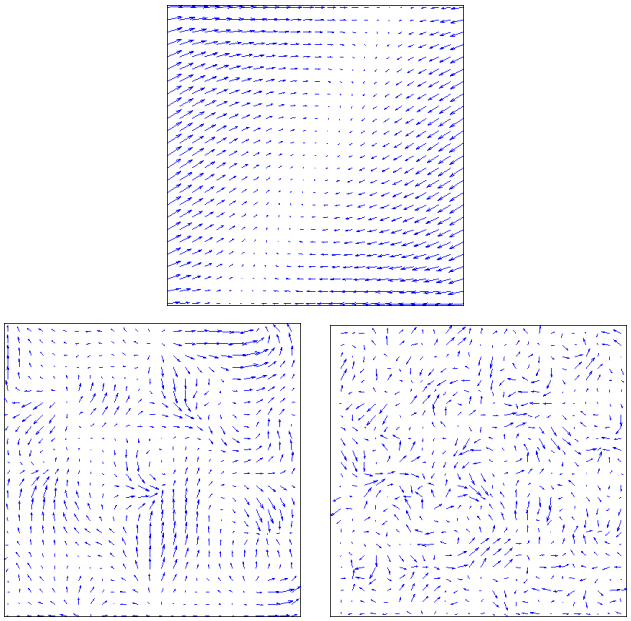

Figure 4. The components of the flow u from Fig. 2: u^c (top), u^s (bottom, left), and u^t (bottom, right). The vectors of u^s, u^t are scaled-up for better visibility. Note that despite $|u| \approx |u^c|$, structural and texture part u^s and u^t are recovered well.

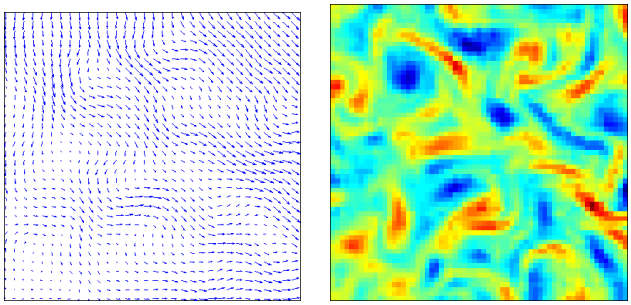

Figure 5. Ground truth data u and its curl to be estimated from a corresponding artificially created image sequence. u is a superposition of a laminar flow (div- and curl-free) and turbulent vortices.

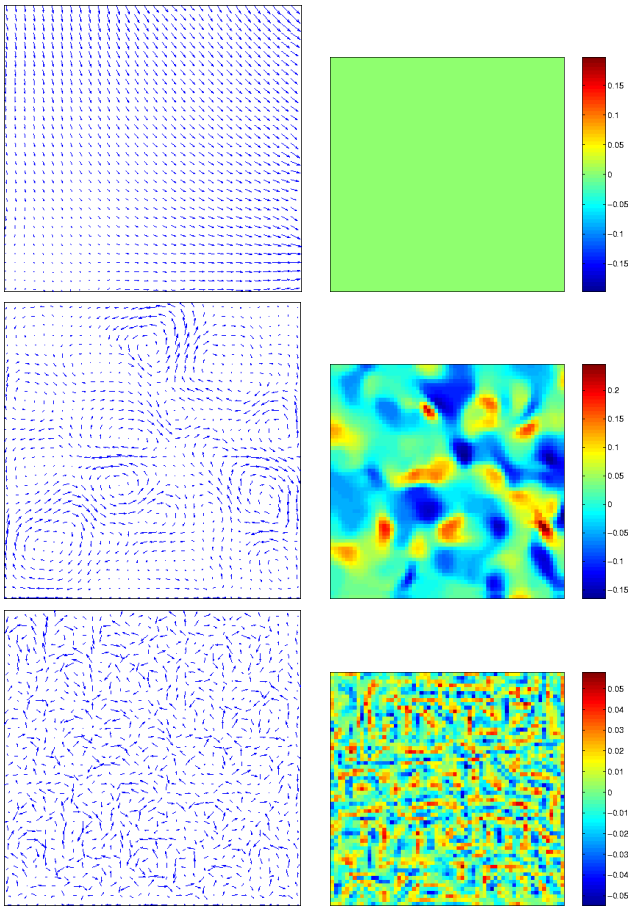

Figure 6. Estimated and decomposed flow corresponding to Fig. 5, using the approach (14). From top to bottom: u^c, ω^c, u^s, ω^s, and u^t, ω^t. Note, that the laminar component is almost completely represented by u^c, ω^c, whereas the turbulent patterns are captured by the remaining components at two different scales. The texture components u^t, ω^t reflect the lack of robustness of G-norm regularization in combination with the degenerate data term for optical flow estimation.

sented a variational model for the decomposition-based estimation of divergence-free flows which is of interest for experimental fluid dynamics. Numerical results conducted by convex second-order cone programming showed the feasibility of our approach as well as promising results with respect to the processing and analysis of complex flow patterns in real-world applications.

Our further work concerns the study of various TV $-$ $*$ combinations of regularizers for flow field decomposition which in comparison to image decomposition may behave differently due to the data term and corresponding image pre-processing. Furthermore, we will investigate more robust models for using G-norm regularization in connection with the (mathematically) degenerate data term for optical flow estimation.

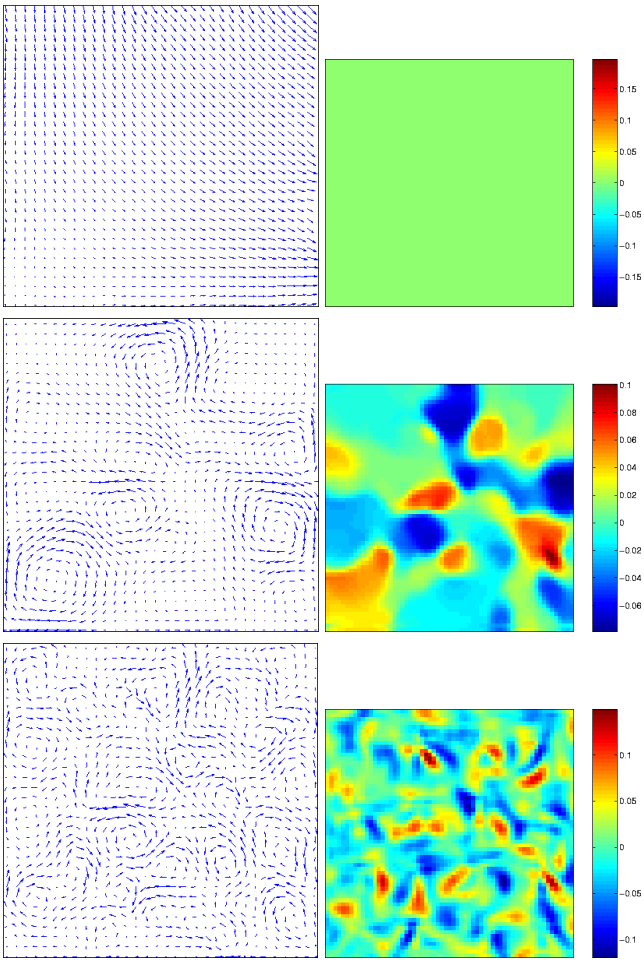

Figure 7. Results analogous to Fig. 6, computed with $TV - L_2$ regularization (15), however. The sensitivity of the texture part (bottom row) has been removed.

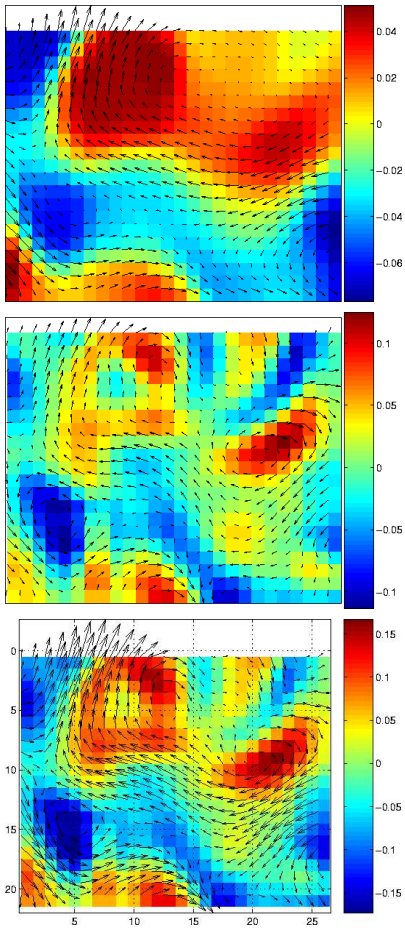

Figure 8. Close-up view of a section of Fig. 7. From top to bottom: $\omega^s, \omega^t, \omega^s + \omega^t$ with the corresponding flows as overlays.

7. Appendix

Let our primal grid consist of $m \times n$ vertices. Reshaping the scalar/vector fields columnwise into vectors, we can identify

$$H_P = \mathbb{R}^{mn},\ H_P^o = \mathbb{R}^{(m-2)(n-2)}, H_V = \mathbb{R}^{(n-1)(n-1)},$$

$$H_S = \mathbb{R}^{m(n-1)+n(m-1)}, H_S^o = \mathbb{R}^{(m-1)(n-2)+(n-1)(m-2)},$$

and finally H_E, H_E^o as H_S, H_S^o. While H_P and H_V are equipped with the usual Euclidian norm, the norm on H_S and H_E^o are given cell adapted as follows: for $u \in H_S$ and $i = 1, \dots, m-1; j = 1, \dots, n-1$, let

$$u_{V_{i,j}} := \frac{1}{\sqrt{2}} \left(u_{i,j+\frac{1}{2}}, u_{i+1,j+\frac{1}{2}}, u_{i+\frac{1}{2},j}, u_{i+\frac{1}{2},j+1}\right)^{\mathrm{T}}.$$

and

$$\|u\|_{H_S}^2 := \sum_{i=1}^{m-1} \sum_{j=1}^{n-1} \|u_{V_{i,j}}\|_2^2$$
$$= \sum_{i=1}^{m-1} \sum_{j=1}^{n-1} \frac{1}{2}(u_{i,j+\frac{1}{2}}^2 + u_{i+1,j+\frac{1}{2}}^2 + u_{i+\frac{1}{2},j}^2 + u_{i+\frac{1}{2},j+1}^2).$$

Similarly, we introduce the norm on H_E^o with respect to $u_{P_{i,j}^o}$. Further we define the TV functional for $\rho \in H_V$ as $\mathrm{TV}(\rho) := |\overline{\mathbb{G}}\,\rho|_{H_S}$, where

$$|u|_{H_S} = \sum_{i=1}^{m-1} \sum_{j=1}^{n-1} \|u_{V_{i,j}}\|_2$$
$$= \sum_{i=1}^{m-1} \sum_{j=1}^{n-1} \sqrt{\frac{1}{2}(u_{i,j+\frac{1}{2}}^2 + u_{i+1,j+\frac{1}{2}}^2 + u_{i+\frac{1}{2},j}^2 + u_{i+\frac{1}{2},j+1}^2)}$$

and for $\omega \in H_P^o$ as $\mathrm{TV}(\omega) := |\mathbb{G}|_{H_P^o}\, \rho|_{H_E^o}$. Finally, the discrete G norms are given by

$$\begin{aligned} \|\rho\|_G &:= \inf_{\rho=\mathbb{D}iv\ p} \| \left(\|p_{V_{i,j}}\|_2 \right)_{i,j} \|_\infty, \\ \|\omega\|_G &:= \inf_{\omega=\mathbb{D}iv\ p} \| \left(\|p_{P^o_{i,j}}\|_2 \right)_{i,j} \|_\infty. \end{aligned}$$

Let

$$\boldsymbol{D}_m := \begin{pmatrix} -1 & 1 & 0 & \dots & 0 & 0 & 0 \\ 0 & 1 & -1 & \dots & 0 & 0 & 0 \\ & & \ddots & \ddots & \ddots & & \\ & & & \ddots & \ddots & & \\ 0 & 0 & 0 & \dots & -1 & 1 & 0 \\ 0 & 0 & 0 & \dots & 0 & -1 & 1 \end{pmatrix} \in \mathbb{R}^{m-1,m},$$

$$\tilde{\boldsymbol{D}}_m := \begin{pmatrix} 2 & 0 & 0 & \dots & 0 & 0 & 0 \\ -1 & 1 & 0 & \dots & 0 & 0 & 0 \\ 0 & 1 & -1 & \dots & 0 & 0 & 0 \\ & & \ddots & \ddots & \ddots & & \\ & & & \ddots & \ddots & & \\ 0 & 0 & 0 & \dots & -1 & 1 & 0 \\ 0 & 0 & 0 & \dots & 0 & -1 & 1 \\ 0 & 0 & 0 & \dots & 0 & 0 & -2 \end{pmatrix} \in \mathbb{R}^{m+1,m},$$

Then the discrete first order operators can be identified with the following matrices:

$$\begin{aligned} \mathbb{G} &= \begin{pmatrix} \boldsymbol{I}_n \otimes \boldsymbol{D}_m \\ \boldsymbol{D}_n \otimes \boldsymbol{I}_m \end{pmatrix}, \quad \overline{\mathbb{G}} = \begin{pmatrix} \boldsymbol{I}_{n-1} \otimes \tilde{\boldsymbol{D}}_{m-1} \\ \tilde{\boldsymbol{D}}_{n-1} \otimes \boldsymbol{I}_{m-1} \end{pmatrix}, \\ \mathbb{D}iv &= \begin{pmatrix} \boldsymbol{I}_{n-1} \otimes \boldsymbol{D}_m, \boldsymbol{D}_n \otimes \boldsymbol{I}_{m-1} \end{pmatrix}, \\ \overline{\mathbb{D}iv} &= \begin{pmatrix} \boldsymbol{I}_{n-2} \otimes \boldsymbol{D}_{m-1}, \boldsymbol{D}_{n-1} \otimes \boldsymbol{I}_{m-2} \end{pmatrix}, \\ \mathbb{C}url &= \begin{pmatrix} \boldsymbol{D}_n \otimes \boldsymbol{I}_{m-1}, -\boldsymbol{I}_{n-1} \otimes \boldsymbol{D}_m \end{pmatrix}, \\ \overline{\mathbb{C}url} &= \begin{pmatrix} \boldsymbol{D}_{n-1} \otimes \boldsymbol{I}_{m-2}, -\boldsymbol{I}_{n-2} \otimes \boldsymbol{D}_{m-1} \end{pmatrix}, \end{aligned}$$

where $\otimes$ denotes the Kronecker product of matrices. The operator $\mathbb{G}^\perp : H_P \to H_S$ is defined by

$$\mathbb{G}^\perp = \begin{pmatrix} -\boldsymbol{D}_n \otimes \boldsymbol{I}_m \\ \boldsymbol{I}_n \otimes \boldsymbol{D}_m \end{pmatrix}.$$

It is easy to check that the restricted operator $\mathbb{G}^\perp|_{H_P^o}$ maps to H_S^o. Finally, the boundary operators are given by

$$\mathbb{B}_{\mathrm{n}} = \begin{pmatrix} \boldsymbol{I}_{n-1} \otimes \boldsymbol{B}_m & \boldsymbol{0} \\ \boldsymbol{0} & \boldsymbol{B}_n \otimes \boldsymbol{I}_{m-1} \end{pmatrix},$$

where $\boldsymbol{0}$ are zero matrices of appropriate sizes and

$$\boldsymbol{B}_m := \begin{pmatrix} -1 & 0 & \dots & 0 & 0 \\ 0 & 0 & \dots & 0 & 1 \end{pmatrix} \in \mathbb{R}^{2,m}.$$

References

[1] J. Aujol, G. Aubert, L. Blanc-Féraud, and A. Chambolle. Image decomposition into a bounded variation component and an oscillating component. *J. of Math. Imag. Vision*, 22(1):71–88, 2005.

[2] J. Aujol and A. Chambolle. Dual norms and image decomposition models. *Int. J. of Comp. Vision*, 63(1):85–104, 2005.

[3] J.-F. Aujol and A. Chambolle. Dual norms and image decomposition models. *International Journal of Computer Vision*, 63(1):85 – 104, 2005.

[4] J.-F. Aujol, G. Gilboa, T. Chan, and S. Osher. Structure-texture image decomposition - modeling, algorithms, and parameter selection. Cam report 05-10, UCLA, 2005.

[5] T. Corpetti, E. Mémin, and P. Pérez. Dense estimation of fluid flows. *IEEE Trans. Patt. Anal. Mach. Intell.*, 24(3):365–380, 2002.

[6] J. M. Hyman and M. J. Shashkov. Adjoint operators for the natural discretizations of the divergence, gradient and curl on logically rectangular grids. *Appl. Numer. Math.*, 25(4):413–442, 1997.

[7] J. M. Hyman and M. J. Shashkov. Natural discretizations for the divergence, gradient, and curl on logically rectangular grids. *Comput. Math. Appl.*, 33(4):81–104, 1997.

[8] J. M. Hyman and M. J. Shashkov. The orthogonal decomposition theorems for mimetic finite difference methods. *SIAM J. Numer. Anal.*, 36(3):788–818 (electronic), 1999.

[9] T. Kohlberger, E. Mémin, and C. Schnörr. Variational dense motion estimation using the helmholtz decomposition. In L. Griffin and M. Lillholm, editors, *Scale Space Methods in Computer Vision*, volume 2695 of *LNCS*, pages 432–448. Springer, 2003.

[10] J. Lewalle, J. Delville, and J.-P. Bonnet. Decomposition of mixing layer turbulence into coherent structures and background fluctuations. *Applied Scientific Research*, 64(4):301–328, 2000.

[11] M. S. Lobo, L. Vandenberghe, S. Boyd, and H. Lebret. Applications of second-order cone programming. *Linear Algebra and its Applications*, 1998.

[12] Y. Meyer. *Oscillating patterns in image processing and nonlinear evolution equations*, volume 22 of *University Lecture Series*. American Mathematical Society, Providence, RI, 2001. The fifteenth Dean Jacqueline B. Lewis memorial lectures.

[13] H. Mittelmann. An independent benchmarking of SDP and SOCP solvers. *Math. Programming, Series B*, 95(2):407–430, 2003.

[14] M. Raffel, C. Willert, and J. Kompenhans. *Particle Image Velocimetry*. Springer, 2nd edition, 2001.

[15] L. Rudin, S. Osher, and E. Fatemi. Nonlinear total variation based noise removal algorithms. *Physica D*, 60:259–268, 1992.

[16] D. Suter. Motion estimation and vector splines. In *Proceedings of the Conference on Computer Vision and Pattern Recognition*, pages 939–942, Los Alamitos, CA, USA, June 1994. IEEE Computer Society Press.

[17] L. Vese and S. Osher. Modeling textures with total variation minimization and oscillating patterns in image processing. *J. Scient. Computing*, 15:553–572, 2003.

[18] L. Vese and S. Osher. Image denoising and decomposition with total variation minimization and oscillatory functions. *J. of Math. Imag. Vision*, 20(1/2):7–18, 2004.

[19] W. Yin, D. Goldfarb, and S. Osher. Total variation based image cartoon-texture decomposition. Technical Report CORC TR-2005-01, Columbia University, 2005. submitted to *Inverse Problems*.